Journal of Applied Polymer Science

Hemostatic activities of nano/microporous bilayer dressings in a femoral artery bleeding rat model

Zeynep Karahaliloğlu,[1] Murat Demirbilek,[2] İbrahim Ulusoy,[3] Berrak Gümüşkaya,[4,5] Emir Baki Denkbaş[6]

[1]Biology Division, Aksaray University, Aksaray 68100, Turkey
[2]Advanced Technologies Research and Application Center, Hacettepe University, Beytepe, Ankara 06800, Turkey
[3]Adacell, Yıldırım Beyazıt Training and Research Hospital, Dışkapı, Ankara 06110, Turkey
[4]Faculty of Medicine, Yıldırım Beyazıt University, Bilkent Ankara 06800, Turkey
[5]Department of Pathology, Atatürk Training and Research Hospital, Bilkent, Ankara 06800, Turkey
[6]Department of Chemistry, Biochemistry Division, Hacettepe University, Beytepe, Ankara 06800, Turkey
Correspondence to: E. Baki Denkbaş (E-mail: emirdenkbas@gmail.com)

ABSTRACT: Recently, an effective hemostatic dressing requirement has become a major problem in both the military and civilian world. Available hemostatic agents are too expensive, ineffective, unsafe, or complicated to use. Here, we evaluated the hemostatic efficacy of a nano/micro bilayer hemostatic dressing including a porous sublayer from chitosan (CTS) and bacterial cellulose (BC) and a nanofibrillar upper layer from silk fibroin (SF). In addition, several active agents rolled in coagulation cascade [vitamin K (Vit K), protamine sulfate (PS), kaolin (Kao), etc.] were doped to the sublayer of bilayer hemostatic agent and their activities were compared via *in vivo* and *in vitro* tests. Lactate dehydrogenase (LDH) activity test results demonstrated that BC/CTS, SF-coated BC/CTS, and Vit K K/BC/CTS, SF/phosphatidylcholine (PC)-coated BC/CTS showed higher LDH activity compared to standard gauze ($p < 0.005$). In a femoral artery bleeding rat model, SF-coated PS/BC/CTS significantly reduced bleeding time (80 ± 0.3 s) compared to standard gauze and kaolin-doped group ($p < 0.005$). Blood loss and mortality rate with 2.3 g and 37.5% SF-coated BC/CTS and SF-coated PS/BC/CTS showed increased efficacy in achieving hemostasis compared to standard gauze. All the prepared hemostatic dressings except for kaolin-doped BC/CTS and standard gauze induced no inflammatory reaction in the tissue. All these data suggest that active agent-doped BC/CTS/SF-based bilayer hemostatic dressings have a great influence on the resulting hemostatic action. © 2016 Wiley Periodicals, Inc. J. Appl. Polym. Sci. **2016**, *133*, 43657.

KEYWORDS: biomaterials; biomedical applications; composites; electrospinning; fibers

Received 4 November 2015; accepted 16 March 2016
DOI: 10.1002/app.43657

INTRODUCTION

Uncontrolled hemorrhage is reported as the most common cause of deaths and injuries in traumatic patients.[1–3] Hence, the early identification and control of bleeding is a crucial step in first aid and postsurgery because intraoperative blood loss increases the incidence of postoperative morbidity and mortality.[4,5] Numerous methods have been used to achieve hemostasis. In the last decade, various effective hemostatic agents have been designed in conjunction with conventional hemostatic techniques such as cauterization,[6] direct pressure,[7] and ligation.[8] These effective hemostatic agents include biological and synthetic topical agents such as gelatin products, oxidized cellulose, microfibrillar collagen, topical thrombin, fibrin sealants, and platelet gels which are commercially available. However, they have some limitations, such as they may induce allergic reactions and unknown infectious diseases as well as having opaque properties as observed in powder-type topical hemostatic agents.[9,10]

To overcome these limitations, nanotechnology presents new possibilities in medical technology. It has also been reported that hemostatic agents produced without using nanotechnology show a weak cationic bonding property and do not activate the platelets effectively.[11,12] Recently, a new nanotechnological approach, the self-assembly of synthetic peptide into a nanofibrous network, was used to generate rapid hemostasis. Although promising results are obtained through this method, difficulties occur during synthesis of peptides and cost overrun limit its use.[13–15] Therefore, the current requirement is an inexpensive nano/microhemostatic agent based on widely available materials which will enable medical technology to avoid the expensive synthetic peptides which are difficult to synthesize.

HemCon and Quikclot available on the market display a good performance in both laboratory trials and field applications. Hemcon is a chitosan (CTS)-based hemostatic agent and works by cross-linking red blood cells to form a mucoadhesive barrier.[16,17] One of the most attractive hemostatic agents is Quikclot, which contains a synthetic zeolite 5A with LTA structure and works through rapid absorption of blood water content as factor concentrators as well as promoting the agglutination of cellular and protein components of blood.[18] However, these commercial products have a critical disadvantage such as nonconformity for deep and narrow wounds and cause tissue injury due to the great exothermic reaction.[18,19] Based on these limitations, our discovery introduces a new porous bilayer hemostatic agent to stop bleeding. This is achieved through the use of nanotechnology consisting of a nanofibrillar barrier and basement-incorporated procoagulants which activate the clotting cascade or deliver clotting factors). An important factor is that the basement-incorporated procoagulants are based on widely available, inexpensive materials, namely, CTS and cellulose.[20,21]

In this study, we examined the use of a functional nano/micro double layer blood-stopping dressing to provide a rapid hemostasis. In the first instance, the sublayer of hemostatic dressings was prepared from cellulose and CTS that are frequently used in the medical industry. Thereafter, hemostatic active agents (calcium ions, vitamin K, kaolin, etc.) which play an active role in the coagulation cascade were incorporated into the structure of the hemostatic dressings. At this point, the doped hemostatic agents serve in the induction of the coagulation cascade, i.e., as a procoagulant. In the sublayer of hemostatic dressings, CTS works as a mucoadhesive agent while bacterial cellulose (BC) has a role in the water absorption of blood. The upper nanofibrillar layer from SF or PC accelerates thrombocyte migration due to the similarity of the nanofibrillar structure to collagen/elastin fibers in the extracellular matrix and its high surface area/volume ratio. Furthermore, we here projected that the doping of kaolin into the BC/CTS hemostatic dressings reduces the generated heat at wound interface. As a result, in this study, we aimed to increase the clotting power of the fabricated nano/micro double layer BC/CTS hemostatic dressings by activating more than one mechanism.

The performances of the doped bilayer nano/micro dressing with different hemostatic active agents were investigated comparatively by *in vitro* and *in vivo* coagulation tests within the scope of this study. The amount of adhered thrombocyte on the hemostatic dressings was compared using lactate dehydrogenase (LDH) assay and SEM images. The coagulation time of blood, total blood loss, and mortality rate of groups were compared in a femoral artery bleeding rat model.

EXPERIMENTAL

Materials

Acetobacter xylinum ATCC 10245 obtained from the American Type Culture Collection (USA) and Hestrin–Schramm (HS) medium[22] were used for BC production. Low-molecular-weight CTS (with degree of deacetylation about 75–85%) and kaolin (aluminum silicate hydroxide) were purchased from Sigma-Aldrich. Protamin HCl (1000 IU mL^{-1}) and vitamin K (Konakion, 10 mg mL^{-1}) were used in the preparation of hemostatic agents.

Silk cocoons of *Bombyx mori* were obtained from Kozabirlik, Turkey. The chemicals used for the preparation of the spinning solutions, trifluoroacetic acid, and calcium chloride were obtained from Sigma, Germany.

The ethics committee of Yıldırım Beyazıt Training and Research Hospital approved the study. This study was conducted as an experimental research in Cell Therapy, Regenerative Medicine and Genomics Research and Application Center (Adacell). *In vitro* and *in vivo* coagulation tests were studied using arterial blood of Sprague–Dawley rats collected in siliconized tubes containing 3.8% sodium citrate.

Production of BC Membrane

Acetobacter xylinum ATCC 10245 obtained from the American Type Culture Collection (USA) was cultivated in a medium containing 25 g glucose L^{-1}, 3 g peptone L^{-1}, and 5 g yeast extract L^{-1} (pH 5) for 24 h at 30 °C in dynamic culture at 4 g. Then, the *A. xylinum* bacteria were inoculated in a polymer medium including 20 g glucose L^{-1}, 10 g peptone L^{-1}, 10 g yeast extract L^{-1}, 8 m*M* of KH_2PO_4, and 12 m*M* of K_2HPO_4 and cultivated for 7 days at 30 °C in static culture. BC membranes were harvested and cleaned by immersion in NaOH solution of 0.1 *M* at 80 °C for 1 h. The membranes were washed with deionized water.

The surface morphology of microfibrillated BC membrane was characterized using a scanning electron microscopy (SEM, JEOL JSM700F) and an atomic force microscopy (AFM, High Performance AFM Head, Nanomagnetics, Turkey). The image was obtained in tapping mode using silicon cantilever with spring constant of 1–5 N m^{-1} and tip radius curvature of 5–10 nm.

Preparation of Sublayer Including BC/CTS of Hemostatic Dressings

Native and active agent-doped BC/CTS hemostatic dressings were prepared by using a homogenizer (IKA, Digital Disperser/Homogenizer System Ultra-Turrax T18). Briefly, BC was suspended in 2% (w/v) CTS solutions dissolved in 1% solution of acetic acid (v/v). After the homogenization procedure, a native BC/CTS hemostatic dressing was prepared by the addition of 0.5 g of $CaCl_2$. Active agent-doped BC/CTS dressings were fabricated by the addition of active agents in coagulation cascade (kaolin, vitamin K, and protamine sulfate (PS) to the aforementioned BC/CTS/$CaCl_2$ mixture. The compositions of native and composite hemostatic dressings were described in detail in Table I. The samples were cooled to a temperature of −80 °C (Revco ULT390–5-V31, USA) and the suspension was allowed to freeze. The frozen hemostatic agents were placed into a freeze-drying vessel (CHRIST ALPHA 2-4LD, Germany) at a preset temperature of −70 °C. The hemostatic dressings were freeze-dried for 24 h to remove the water phase completely.

Epichlorohydrin (ECH) was used to increase the stability of CTS in water. The sublayer of the prepared hemostatic dressings was cross-linked at a reaction temperature of about 70 °C under ECH vapor. The effect of the cross-linking reaction of BC/CTS hemostatic dressings was determined by Fourier-transformed

Table I. Native and active agent doped BC/CTS hemostatic agents components

Experimental groups	CTS (mL)	BC (g)	$CaCl_2$ (g)	Kaolin (g)	Vitamin K (mg)	Protamine Sulfate (IU)
BC/CTS	7	14	0.5			
SF coated BC/CTS	7	14	0.5	-	-	-
SF/PC coated BC/CTS	7	14	0.5	-	-	-
SF coated Kao/BC/CTS	7	14	0.5	1		-
SF coated Vit K/BC/CTS	7	14	0.5	-	10	-
SF coated PS/BC/CTS	7	14	0.5	-	-	1000

infrared spectroscopy (Perkin Elmer SpectrumOne, Nicolet 520, USA). The spectra were recorded over the range of 500–4000 cm^{-1}.

The surface morphologies of freeze-dried native and active agent-doped BC/CTS hemostatic dressings were characterized using SEM (JEOL JSM700F). For further examination of the composite BC/CTS hemostatic dressings, samples were immersed in liquid nitrogen for 10 min and then the samples were cut using a sharp blade along their cross-sections. The hemostatic dressings were coated with gold with a sputter coater at 15 kV for 5 min and characterized using SEM.

Preparation of the Upper Layer Including Silk Fibroin (SF) or SF/Phosphatidylcholine (PC) of Hemostatic Dressings by Electrospinning

Prior to the electrospinning process, raw silk cocoons was degummed with 0.05 *M* of disodium carbonate for 30 min to extract the glue-like sericin coating layer from the structural fibroin protein. The obtained SF fibers were dried overnight at 40 °C. SF solution was prepared by dissolving the degummed silk fibers in trifluoroacetic acid. The concentration of SF in trifluoroacetic acid was 12.5% (w/v). As an experimental group, the SF/PC blend was mixed in the ratio of 2:1 (w/w) to prepare SF/PC-coated BC/CTS hemostatic dressings. All solutions were magnetically stirred and held at room temperature.

A typical electrospinning setup which includes a high-voltage supply (Spellman CZE1000R, Germany), syringe pump (Harvard Apparatus 11 Plus), and a metallic collector was used in this study. SEM (JEOL JSM700F) was used for observing the morphology of electrospun SF and SF/PC upper layer of hemostatic agents. The average fiber diameter was determined by measuring diameters of fibers at 500 points from approximately 8 images taken per area using image-processing software (ImageJ, NIST).

Water-Uptake Properties of Bilayer BC/CTS Hemostatic Dressings

The swelling behavior of bilayer BC/CTS hemostatic dressing was determined using a phosphate buffer solution (PBS). Briefly, freeze-dried BC/CTS hemostatic dressings with known weight (W_{dry}) were immersed in 10 mL of PBS solution, pH 7.4 at 37 °C. The solution was renewed after every measurement. At regular intervals, the hemostatic dressings were taken out of PBS and excess solutions were removed with a filter paper. The weight of the hemostatic scaffolds was measured (W_{wet}). The swelling degree of the hemostatic dressings in PBS was calculated as

$$W = \left(W_{dry} - W_t\right)/W_{dry} X\ 100$$

where *W*, W_{dry}, and W_t represent the absorbability percent of PBS, initial weight, and weight at time *t*, respectively. The values were expressed as the means with standard deviation ($n = 3$).

LDH Activity of Bilayer BC/CTS Hemostatic Dressings

LDH activity of bilayer BC/CTS hemostatic dressings was determined using an LDH/LD Kit (Sigma-Aldrich, USA). Arterial blood from rats was collected in siliconized tubes containing 3.8% sodium citrate and platelet-rich plasma (PRP) was obtained by centrifugation at 3000 *g* for 10 min. The prepared hemostatic dressings were incubated at 37 °C for 1 h in PRP of 1 mL. The samples were rinsed in PBS to remove nonadherent platelets. The adhered platelets on hemostatic agents were lysed using 0.25 mL 1% Triton X-100 in PBS at 37 °C for half an hour. LDH activity was determined by measuring the OD_{450nm} spectrophotometrically (Nanodrop Spectrofotometer, Thermo Sci., USA). Clean standard gauze was used as a control group.

Once prepared, hemostatic dressings were treated with PRP, the samples were fixed with 4% glutaraldehyde solutions for 2 h to scan the platelets adhered onto the hemostatic dressings. The samples were washed with PBS (pH 7.2) and immersed in ethanol solutions (50, 70, 90, 100%, v/v). Finally, hemostatic dressings were treated with hexamethyldisilazane (HMDS) for dehydration and then, the samples were coated with gold/palladium for SEM analysis.

Whole Rat Blood and Plasma Absorption of Bilayer BC/CTS Hemostatic Dressings *In Vitro*

The absorption percentage of hemostatic dressings was determined in whole rat blood and plasma. Sprague–Dawley rat blood and plasma were obtained by the same protocol as described above. To determine the absorption activity, each dried sample was weighed (W_{dry}), 2 mL of the plasma and blood were added dropwise and excess solution was removed with a filter paper and the weight of the hemostatic dressings was measured (W_{wet}). The absorption percent of the samples treated with whole blood and plasma was calculated as follows:

$$\text{Absorption efficiency } (\%) = \left[\left(W_{wet} - W_{dry}\right)/W_{dry}\right] \text{ x100}$$

Where, W_{dry} and W_{wet} represent the initial and final weight of the hemostatic dressings, respectively.

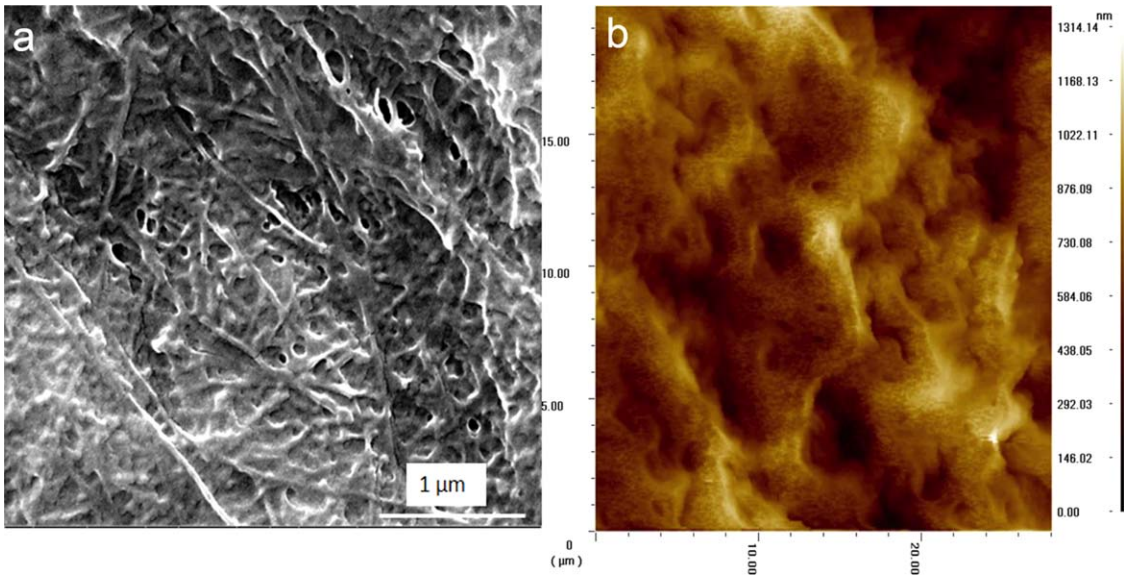

Figure 1. (a) SEM and (b) AFM images of BC membrane. [Color figure can be viewed in the online issue, which is available at wileyonlinelibrary.com.]

Hemostasis in Rat Femoral Artery Model

Fifty-six female Sprague–Dawley rats weighing 250–300 g were purchased from Adacell, Dışkapı Yıldırım Beyazıt Training and Research Hospital. Standard gauze was selected as a control and weighted equally with the other experimental groups. Before animal experiments, the materials were sterilized by UV irradiation for 1 h. All procedures were carried out under sterile conditions.

For the femoral artery model, Sprague–Dawley rats were anesthetized with an intramuscular injection of ketamine and xylazine (2:1 v/v). The body temperature of animals was maintained at $37 \pm 0.5\,^{\circ}C$ during the surgical procedure. Initially, weighed laparotomy pads were placed under the animals to measure blood loss. For mean arterial pressure (MAP) measurements, polyethylene catheters were inserted into the carotid arteries of rats. The femoral artery was punctured using a 24-G cannula needle and allowed a bleeding for 10 s. After uncontrolled hemorrhage, the weighed BC/CTS hemostatic dressings were applied under pressure through the bleeding site by a team member who had no prior knowledge of the composition of the applied hemostatic dressing. BC/CTS hemostatic dressings displayed hemostatic efficiency during the following 5 min period. All animals were monitored during the application of bilayer hemostatic agents. MAP and continuous blood pressure values were recorded by using digital data collection system (Powerlab Bridge Amplifier and Powerlab, AD Instruments, USA). Furthermore, a portable blood gas analyzer (gases: pH, pCO_2, pO_2, BE (ecf), cSO_2; blood chemistry: Na^+, K^+, Ca^+, Cl^-, Hct, cHgb; metabolites: glucose, lactate, creatinine) was used to scan the changes in blood gas parameters during the surgical procedure (Epoc Portable Vet Blood Gas Analyzer, USA). At the group including kaolin, the temperature of hemostasis site was measured using a digital thermometer (Sper Scientific Ltd, 2 Channel Type K/J - 800007). The probe was placed directly to the bottom of the hemostatic agent after the bleeding starts. The temperature probe was connected to a data saving device. The readings were recorded during the surgical procedure.

At the end of the experiment, already weighed laparotomy pads and hemostatic dressings were reweighed for the measurement of the blood loss. The weight difference between before and after hemostasis was recorded as a total blood loss. The mortality rate along 1 h of the femoral artery bleeding rat model was measured and the bleeding times were given for each experimental group. At the end of hemostasis, all animals were sacrificed by overdose ketamine injection.

Histological Examinations

At the end of the experiment, a segment of the femoral artery from the dressing applied area and healthy tissue was obtained. The tissue samples were fixed in 10% formaldehyde solution. From the fixed tissue samples, serial sections were sampled. After the paraffin-embedding procedure, sections from the samples were attached to the slides. Finally, these slides were stained with hematoxylin–eosin (HE) for microscopic imaging and evaluation (Olympus BX51-Floresan). The existence of inflammation was recorded by assessing the HE slides.

Statistical Analysis

Numerical data were analyzed using standard analysis of variance (ANOVA) techniques and statistical difference was considered at $p < 0.005$ and $p < 0.05$. Results were reported as average ± standard error of the mean.

RESULTS AND DISCUSSION

Production and Characterization of BC Membrane

BC membranes were successfully produced by *A. xylinum* in Schramm and Hestrin medium. After purification process, a thin, opaque, white BC membrane was obtained. Figure 1 shows the SEM and AFM images of the produced native BC

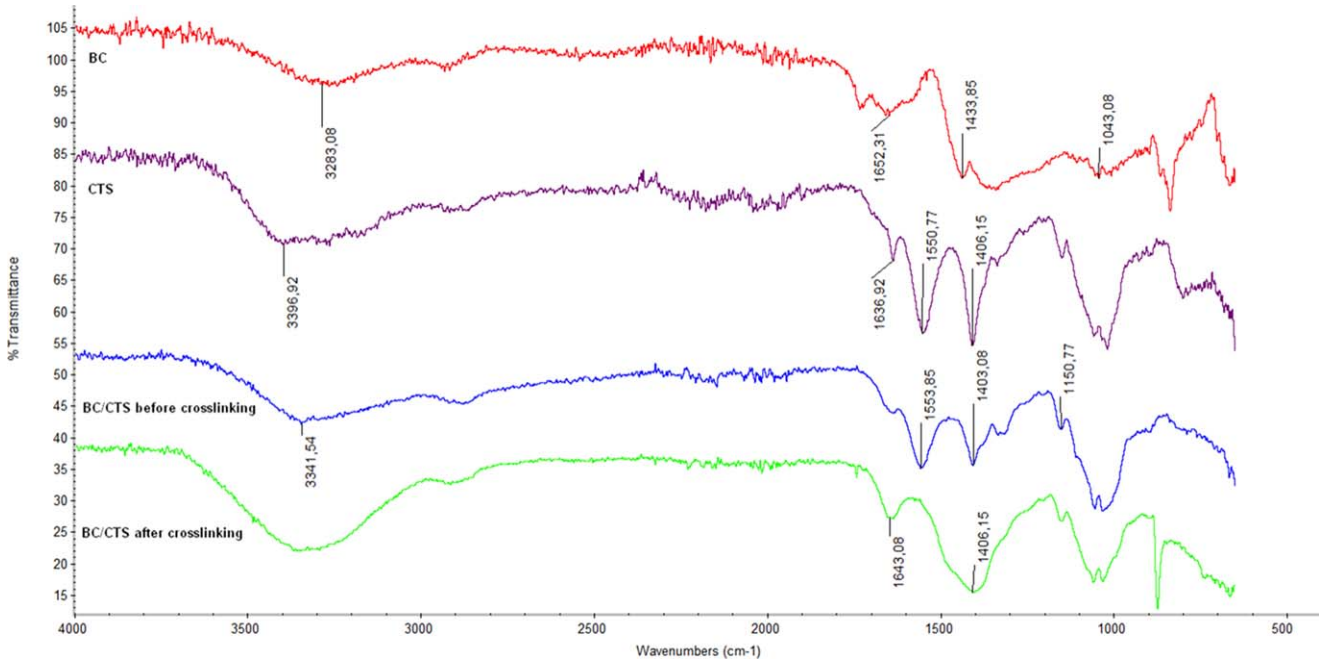

Figure 2. FTIR spectrums of native BC, CTS membrane, and BC/CTS hemostatic dressings before and after cross-linking under ECH vapor. [Color figure can be viewed in the online issue, which is available at wileyonlinelibrary.com.]

membrane. As shown in images, BC exhibited a well-organized three-dimensional network structure with a high surface area.

The interaction between BC and CTS, and the effect of cross-linking by epichlorohydrin on the structure were analyzed in the range between 400 and 5000 cm^{-1} with FTIR analysis. The obtained spectrums were given in Figure 2. The BC showed a strong peak at 3283 cm^{-1} corresponding to —OH stretching. The peaks at 1652 cm^{-1}, 1433 cm^{-1}, and 1043 cm^{-1} corresponding to carboxyl, carbonyl, and C—O—C groups of BC were observed. Sun *et al.* reported that BC produced by *A. xylinum* in Hestrin–Schramm medium showed an absorption band at 3400 cm^{-1}.[23] The observed sharp peak at 1644 cm^{-1} confirmed the presence of carboxyl group in the structure of BC. Furthermore, they attributed to the presence of carbonyl group at the observed peak at 1428 cm^{-1}. The bands at 1163 cm^{-1} and 1068 cm^{-1} were recorded as an indicator of C—O—C function. IR spectrums of the produced BC overlapped with absorption bands of BC in the literature.

Characterization of BC/CTS Hemostatic Dressings

The sublayers of native and active agent-doped BC/CTS hemostatic dressings were fabricated due to a homogenizer. The hemostatic dressings were exposed to ECH vapor at 70 °C overnight to provide the stability of CTS in aqueous media. The IR spectrums before and after cross-linking were compared in Figure 2. CTS shows the absorption bands at 3396 cm^{-1}, 1636 cm^{-1}, 1550 cm^{-1}, and 1406 cm^{1} correspond to O—H and N—H, Amide I, Amide II, and Amide III, respectively.

In the FTIR spectra of BC/CTS, N—H stretching at 3421 cm^{-1} combined with O—H stretching band. As a result of the presence of CTS in structure, new bands were observed at 1632 cm^{-1}, 1553 cm^{-1}, and 1403 cm^{-1} attributed to Amide I, Amide II, and Amide III, respectively.[24] After ECH-cross-linking process, an amine deformation located at 1632 cm^{-1} was showed (shifted to 1643 cm^{-1}) and the increase at C—N stretching (at 1406 cm^{-1}) band was attributed to cross-linking of NH_2 groups in the structure of CTS. Furthermore, the obtained peak at 1085 cm^{-1} corresponding to C—O stretching increased and expanded.[25] These results supported that hydroxyl groups of CTS were cross-linked under high temperature.

Morphological characterization of native BC/CTS hemostatic dressings was carried out using SEM. Figure 3(a) shows an open and interconnected pore morphology of native BC and SEM image of pore wall surface was given in Figure 3(b). The image demonstrates that BC fibrillar structure was well integrated within CTS.

Preparation and Characterization of Upper Layer of BC/CTS Hemostatic Agents

The upper layer of BC/CTS hemostatic dressings was created by electrospinning method. SEM images and fiber diameter distributions of native SF and SF/PC blend nanofibrillar layer were presented in Figure 4. As can be seen in Figure 4, highly uniform and smooth nanofibers without beads were obtained for both structures. The mean fiber diameters for SF and SF/PC blend nanofibrillar layer were found as 450 ± 35 and 750 ± 181 nm, respectively. Fan *et al.* reported similar result for SF scaffolds to investigate the biocompatibility of Schwann cells, which have a fiber diameter of about 400 nm.[26] Mathew *et al.* notified that micellar morphology with diameters on the order of 1–5 μm was obtained by electrospinning of PC solution.[27]

Figure 5 shows the FTIR spectra of SF and SF/PC blend nanofibrillar structure, which is the upper layer of hemostatic dressings. Native SF shows the bands at 1637 cm^{-1}, 1514 cm^{-1}, and

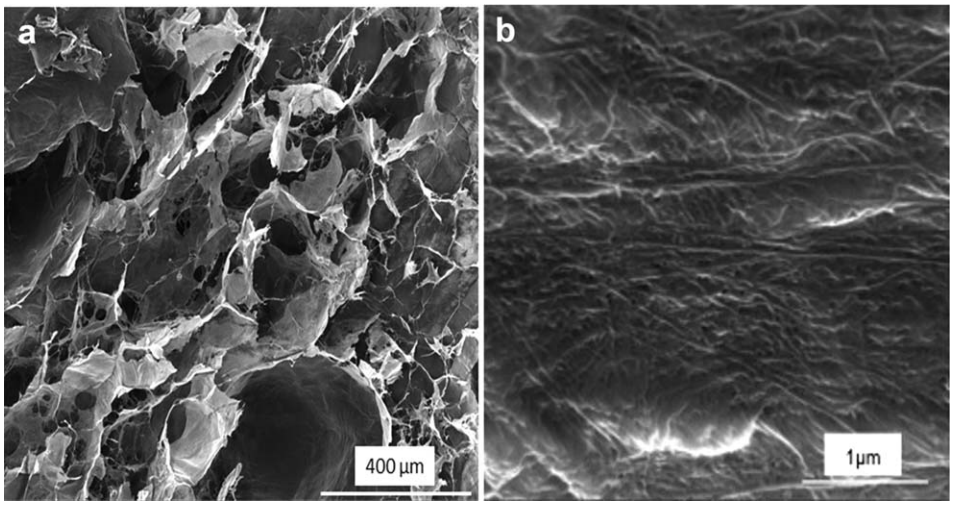

Figure 3. SEM images of native BC/CTS: (a) porous structure; (b) pore wall surface. BC/CTS hemostatic dressings were prepared using a homogenizer and freeze-dried for 24 h to remove the water phase completely (scale bars: 400 and 1 μm).

1231 cm^{-1} attributed to Amide I, II, and III, respectively. The characteristic peaks of SF can be found at 1700–1600 cm^{-1} (Amide I), 1540–1520 cm^{-1} (Amide II), and 1300–1220 cm^{-1} (Amide III) correspond to N—H bending, C—H stretching, and C═O bending, respectively.[28] After blending SF with PC, the obtained spectrum at 2825 and 2851 cm^{-1}, 1234 and 1058 cm^{-1}, 1133 cm^{-1} belong to C—H stretching, PO_2 and CO—O—C groups. The data is similar with the bands of PC in the literature.[29] Furthermore, the specific bands of SF are preserved after blending.

Bilayer structure of active agent-doped hemostatic dressings consisting of nanofibrillar upper and porous sublayer was characterized by SEM. Cross-section and porous sublayer images of active agent-doped hemostatic dressings were presented in Figure 6(a,c,e,g,i and b,d,f,h,j), respectively. The upper nanolayer shows the fibrillar morphology with high surface area while bottom layer exhibits an interconnected, open pore microstructure after freeze-drying. As can be seen in Figure 6, both the layers integrated together without any detachment.

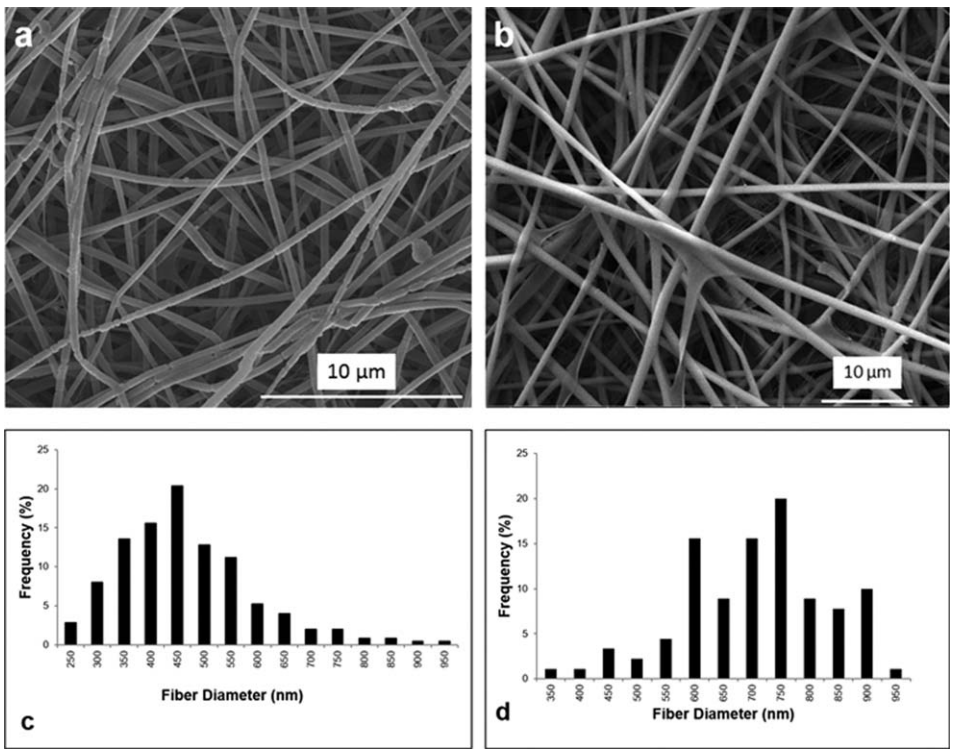

Figure 4. SEM images and fiber diameter distributions of (a,c) native SF and (b,d) SF/PC composite nanofibrillar layer. Electrospinning method was used to prepare native SF or SF/PC upper layer (scale bar: 10 μm). [Color figure can be viewed in the online issue, which is available at www.interscience.wiley.com.]

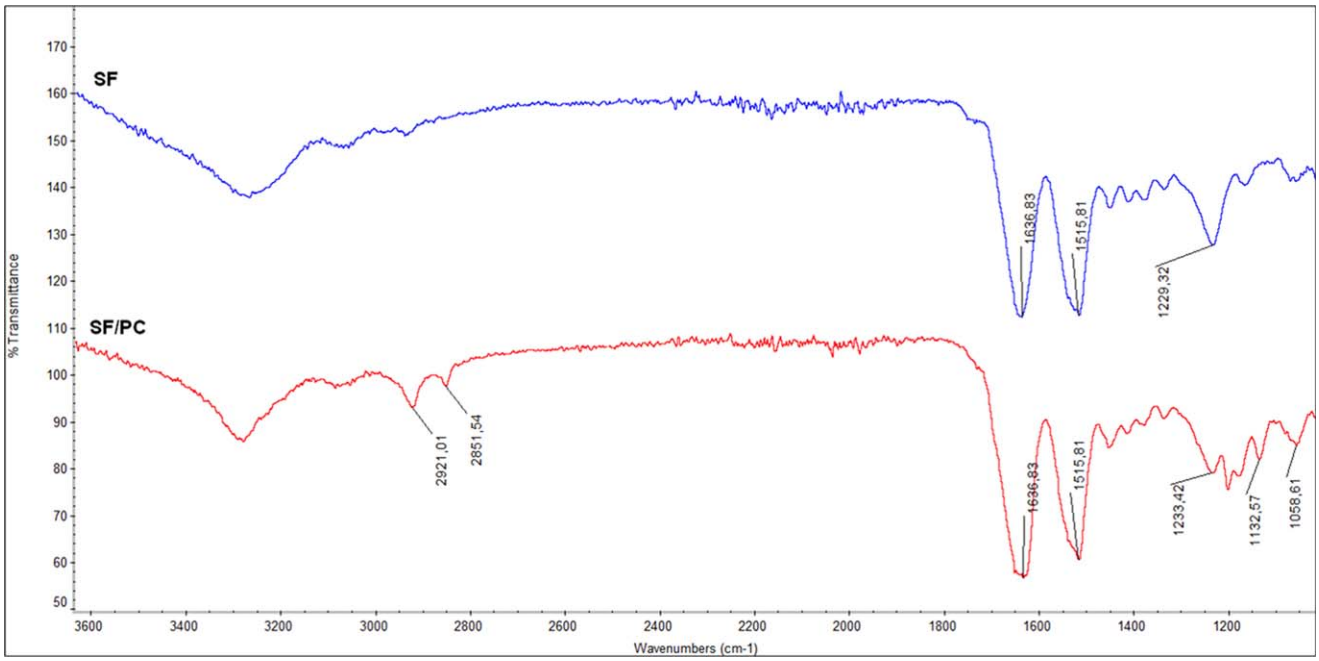

Figure 5. FTIR spectrums of native SF and SF/PC composite nanofibrillar layers. [Color figure can be viewed in the online issue, which is available at wileyonlinelibrary.com.]

Water-Uptake Properties of BC/CTS Hemostatic Dressings

Figure 7 shows the swelling behavior of the native and composite BC/CTS hemostatic dressings during 9 days. At the end of first day, SF-coated BC/CTS, SF-coated PS/BC/CTS, and SF-coated Vit K/BC/CTS showed better water uptake capacity compared to SF-coated Kao/BC/CTS ($p < 0.05$). Similarly, the initial water uptake of BC/CTS scaffold was much higher than that of SF/PC-coated BC/CTS hemostatic dressing ($p < 0.005$). The water-uptake activities of SF-coated Vit K/BC/CTS and PS/BC/CTS were found to be 994% and 1023%, respectively, while were found to be 989% for BC/CTS hemostatic dressings ($p < 0.05$). Furthermore, Kao/BC/CTS were found to have reduced water uptake compared to SF-coated BC/CTS and SF-coated Vit K/BC/CTS and PS/BC/CTS hemostatic dressings.

Hu *et al.* reported that nanoporous bioglass containing silver (*n*-BGS) fabricated by the sol–gel method was reduced the bleeding time in rabbit skin injury models and it was found that the water absorption rate of *n*-BGS was 71%.[30]

Darmoc *et al.* fabricated a hemostatic composition comprising cross-linked collagen and they found that swelling percent of cross-linked fibrillar collagen material (1% microfibrillar collagen, 500:1) was 9.34 ± 1.82%. Furthermore, Floseal® and Surgiflo® competitive products show an average percent swell of about 32% and about 26%, respectively.[31] The results show that BC/CTS hemostatic dressings can absorb a large amount of water compared to counterparts because of its high surface area and porosity.

LDH Activity and Whole Rat Blood and Plasma Absorption of Bilayer BC/CTS Hemostatic Dressings

The LDH activity of the adhered platelets on the BC/CTS hemostatic dressings was measured and so platelet adhesion was determined indirectly. The obtained LDH values after PRP treatment are presented in Figure 8(A). When compared with the standard gauze, the LDH activity of SF/PC-coated BC/CTS and SF-coated Kao/BC/CTS was significantly increased ($p < 0.05$). Also, there is a significant difference in between BC/CTS, SF-coated BC/CTS, SF-coated PS/BC/CTS, SF-coated Vit K/BC/CTS, and standard gauze ($p < 0.005$). Furthermore, SF-coated Vit K/BC/KTS, BC/CTS, and SF-coated BC/CTS show a better LDH activity compared to SF-coated Kao/BC/CTS ($p < 0.005$).

Whole blood and PRP absorptions *in vitro* of bilayer BC/CTS hemostatic dressings are presented in Figure 8(B). Both whole blood and PRP absorption percentage of native and active agent-doped hemostatic dressings was significantly higher compared to standard gauze ($p < 0.05$, $p < 0.005$). In terms of whole-blood absorption, all the fabricated groups are significantly different from kaolin-doped group ($p < 0.05$). The highest absorption ratio was obtained at SF-coated PS/BC/CTS related to whole-blood absorption. The absorption percent for PRP, standard gauze shows minimum performance with 537 ± 51% of absorption rate between all experimental groups. Similar to whole-blood absorption results, SF-coated PS/BC/CTS had the highest PRP absorption capacity.

Dai *et al.* reported that powder form silver exchanged mesoporous silica spheres (AgCaMSS) achieved for rat femoral artery and liver injury model show an absorption rate with 285.2%, whereas granule form reveals with a 198.4%.[32] The trend of all groups regarding to whole-blood and PRP absorption percentage is significantly different compared to counterparts.

The platelets adhered to the surface of native and active agents doped BC/CTS hemostatic dressings during the initial 30 min of incubation were fixed and characterized by SEM as can be seen in Figure 9. Specially, more adhered platelets were observed on the active agent-doped BC/CTS hemostatic dressings compared to SF-coated Kao/BC/CTS.

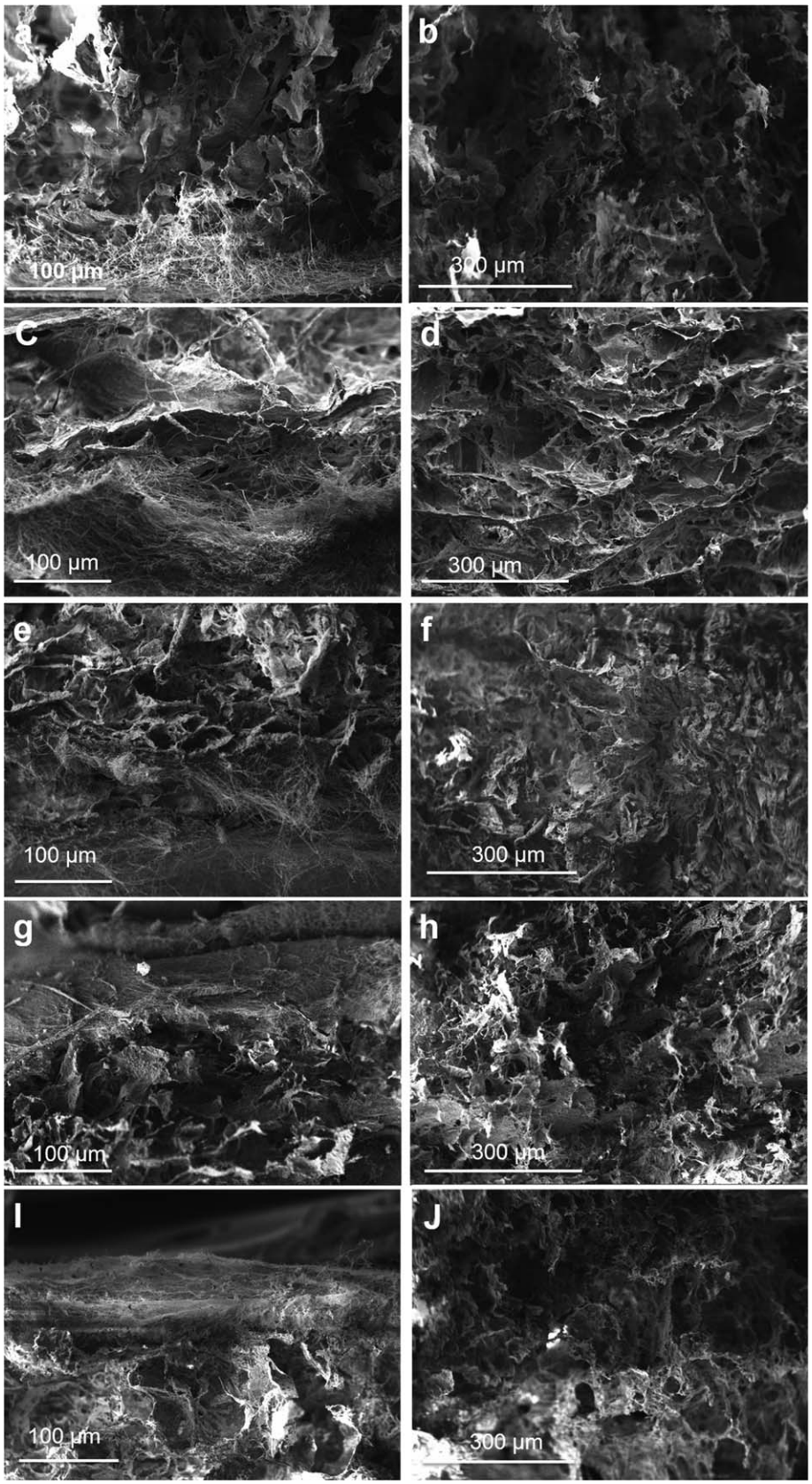

Figure 6. SEM images of (a,b) SF-coated BC/CTS; (c,d) SF/PC-coated BC/CTS; (e,f) SF-coated Kao/BC/CTS; (g,h) Vit K/BC/CTS; and (i,j) PS/BC/CTS hemostatic dressings (left images: bilayer structures, scale bars: 100 μm; right images: sub porous structures, scale bars: 300 μm).

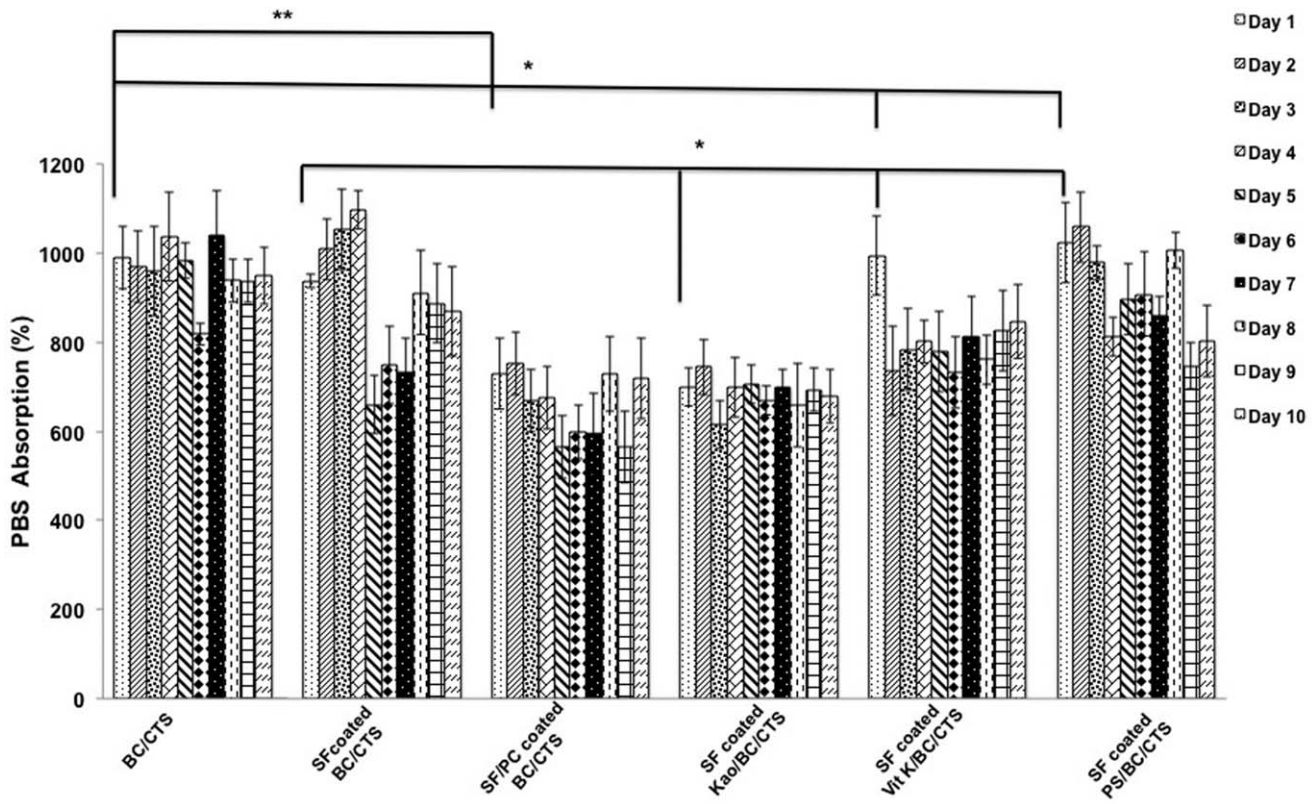

Figure 7. The swelling study of BC/CTS hemostatic dressings. Values are mean ± SEM; $n = 3$.

Hemostasis in a Femoral Artery Bleeding Rat Model

Hemostasis Time and Blood Loss. For femoral artery bleeding rat model, the femoral arteries of rats were surgically exposed and cut. Then, it was treated with native and coagulative agent-doped hemostatic dressings or standard gauze under manual compression. The hemostasis time of different experimental

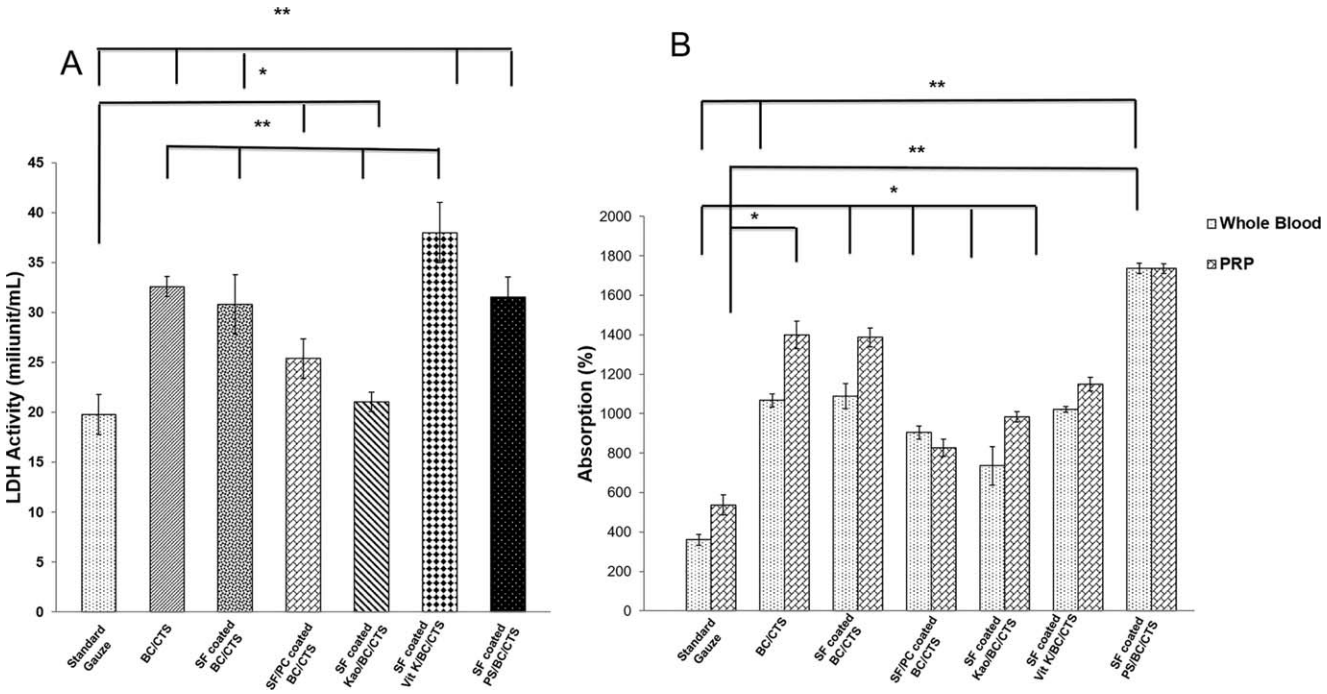

Figure 8. LDH activity results carried out using (A) blood plasma of healthy rats (**$p < 0.005$, *$p < 0.05$) and (B) whole blood and PRP absorption rates of hemostatic dressings (**$p < 0.005$, *$p < 0.05$). Values are mean ± SEM; $n = 3$.

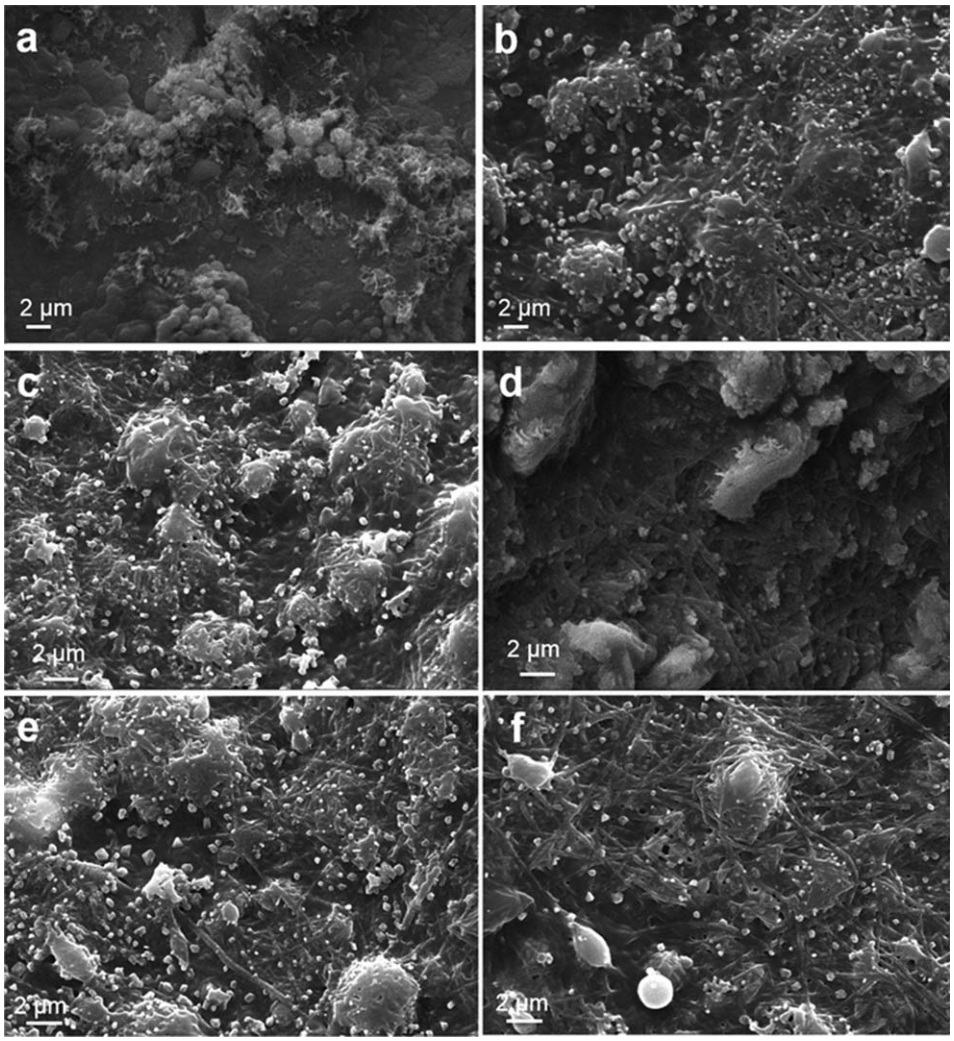

Figure 9. The adhered platelets on hemostatic dressings: (a) BC/CTS , (b) SF-coated BC/CTS, (c) SF/PC-coated BC/CTS, (d) SF-coated Kao/BC/CTS, (e) SF-coated Vit K/BC/CTS, and (f) SF-coated PS/BC/CTS (scale bars: 2 μm).

groups at the bleeding site was recorded and presented in Figure 10(A). Standard gauze stopped the bleeding after 245 ± 4 s. The hemostasis time of native and coagulative agents-doped hemostatic dressings ranged from 80 ± 3 to 180 ± 2 s. When compared with the standard gauze, all BC/CTS hemostatic dressings had significantly better performance ($p < 0.005$). The hemostasis time of SF-coated BC/CTS and PS/BC/CTS was found significantly different than kaolin-doped group. After 80 ± 0.3 s, the hemostasis occurred at SF-coated PS/BC/CTS (less time to hemostasis).

In the study of Hunderson *et al.*, the topical hemostatic agent comprised a PEGylated, polymerized sequence of dihydroxyacetone (MPEG-pDHA) which had a significantly decreased bleeding time (97 s).[33] Sönmez *et al.* reported that APH which is a hemostatic agent with ultrahydrophilic and particulate properties has an effective hemostatic property in rats pretreated or nonpretreated with anticoagulants.[34] It was found that the bleeding time in groups pretreated with warfarin and in the saline administered subgroup were 3.61 and 2.40 min, respectively. When the obtained hemostasis time results with those in literature, the efficiency of the BC/CTS hemostatic dressings proves that the dressings are acceptable in quality for application in the medical industry.

Post-treatment blood loss was determined by measuring the volume of the liquid blood at bleeding site and absorbed blood by hemostatic dressings. Blood loss of the different groups can be seen in Figure 10(B). Native and coagulative agent-doped hemostatic dressings loss significantly less blood than standard gauze ($p < 0.005$). SF-coated BC/CTS and PS/BC/CTS show less blood loss besides shorter hemostasis time.

Nur *et al.* reported that when the gelatin foam prepared by freeze-drying was applied in a rat kidney model, total blood loss was found as 3.02 ± 2.9 g. Similarly, they used commercial SPONGOSTAN® gelatin sponge in a rat kidney hemorrhage model. Average total blood loss (represented as volume $\pm$ SD) was 5.1 ± 1.58 g.[35] Recently, the 1% RADA16-I which is a nanotechnological hemostatic product synthesized by self-assembling showed with 3.22 ± 1.53 g of bleeding loss.[6] We accordingly propose that the hemostatic activity of BC/CTS hemostatic dressings, especially SF-coated BC/CTS and SF-coated PS/BC/

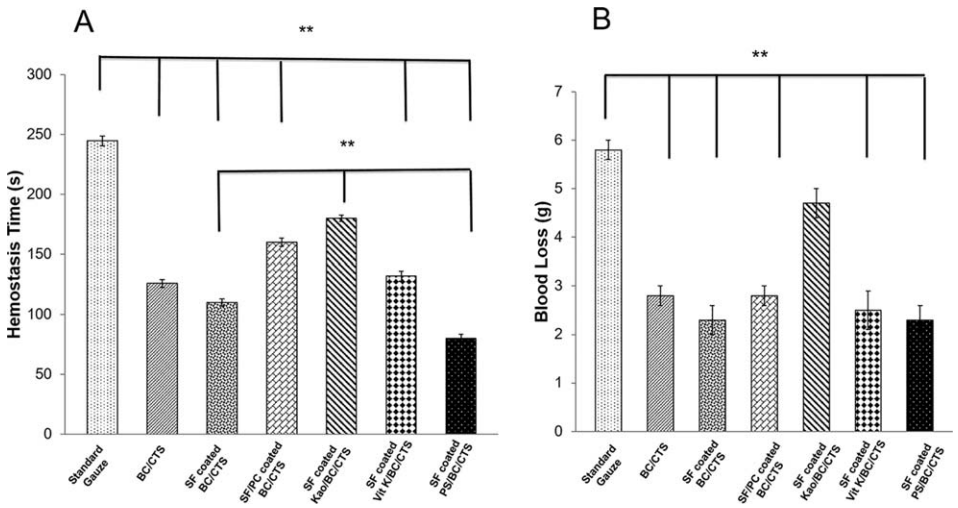

Figure 10. (A) Hemostasis time of hemostatic dressings in a femoral artery bleeding rat model (**$p < 0.005$) and (B) total blood loss in a femoral artery bleeding rat model (**$p < 0.005$). Values are mean ± SEM; $n = 8$.

CTS, have better hemostatic performance compared to the other counterparts.

Mortality and Exothermic Reaction. Mortality rates in different experimental groups after treatment of hemostatic dressings are presented in Figure 11(A). The femoral artery injury resulted in 75% mortality in standard dressing group. BC/CTS, SF-coated BC/CTS, SF-coated Vit K/BC/CTS, and PS/BC/CTS dressings dramatically decreased the mortality to 37.5% (about twofold). Addition of kaolin to BC/CTS hemostatic dressing increased the mortality rate when compared to the other fabricated experimental groups.

Literature reports that the mortality rate for the commercial products such as Celox Gauze and ChitoGauze are 90% and 70%, respectively. Combat Gauze showed a mortality rate of 60%.[36] The application of BC/CTS hemostatic dressings is associated with a mortality rate of 37.5% which is a significant drop from the percentage quoted in literature. Another recent approach for the treatment of injured of injured patients was hemostatic resuscitation using of fresh frozen plasma (FFP). Letourneau *et al.* studied the hemostatic potential of FFP5 group and they found that overall survival was 54%.[37] The results of this study demonstrated that BC/CTS hemostatic dressings has proven itself to be a promising topical hemostatic agent with decreased mortality.

In the femoral artery bleeding model, the exothermic effects of SF-coated Kao/BC/CTS were examined by measuring the temperature at the bleeding site [Figure 11(B)]. The treatment of

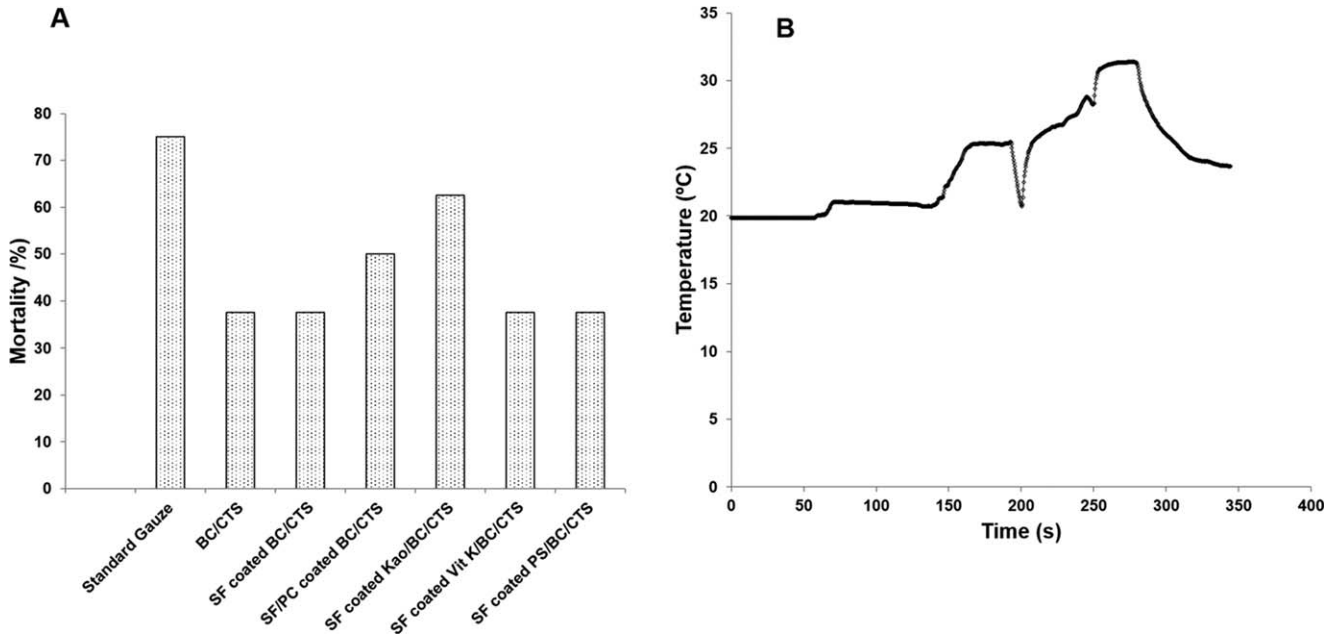

Figure 11. (A) Mortality rate of hemostatic dressings in a femoral artery bleeding rat model and (B) wound temperature after SF-coated Kao/BC/CTS treatment. Values are mean ± SEM; $n = 8$.

Table II. Blood Metabolic Values after Femoral Artery Bleeding Model Created in Healthy Rats

	Metabolites		
Groups	Glu (mg/dL)	Lac (mM)	Crea (μM)
BC/CTS	287.5 ± 0.6	0.865 ± 0.03	33 ± 0.8
SF-coated BC/CTS	226.5 ± 0.3	1.26 ± 0.05	42 ± 0.7
SF/PC-coated BC/CTS	255.5 ± 0.4	0.77 ± 0.2	38.5 ± 0.1
SF-coated Kao/BC/CTS	272.5 ± 0.2	0.78 ± 0.07	24 ± 0.8
SF-coated PS/BC/CTS	337 ± 0.3	1.09 ± 0.1	23.5 ± 0.7
SF-coated Vit K/BC/CTS	268.5 ± 0.1	1.03 ± 0.1	24 ± 0.1
Standard gauze	271 ± 0.1	0.95 ± 0.2	19 ± 0.1

A portable blood gas analyzer was used to scan the changes in blood gas parameters during the surgical procedure.

the kaolin-doped group resulted in a temperature rise of about 10 °C. It is well known that zeolite produces an exothermic reaction and dramatically increases the temperature, causing injury. Another disadvantage is that the agent is difficult to completely remove from the bleeding site and may lead to the formation of inflammation.[38] Arnaud *et al.* investigated the activity of ACS^+ (mineral Al/Si/zeolite) and nine commercial products in a swine-bleeding model. ACS^+ (mineral Al/Si/zeolite) caused a temperature increase of about 7.2 ± 8.7 °C in 2 min.[39] The results obtained in this study verified that alumina-silicate-based hemostatic agents generated heat at the injury site and that the doping of kaolin into the BC/CTS hemostatic dressings had no influence on.

MAP and Blood Gases Analysis. MAPs were measured continuously during rat femoral artery injury model. Baseline MAP were 78.57 ± 11 mmHg for standard gauze, 72.71 ± 13 mmHg for BC/CTS, 58.51 ± 10 mmHg for SF-coated BC/CTS, 71.82 ± 9 mmHg for SF/PC-coated BC/CTS, 85 ± 12 mmHg for SF-coated Kao/BC/CTS, 60.87 ± 13 mmHg for SF-coated Vit K/BC/CTS, and 72.71 ± 10 mmHg for SF-coated PS/BC/CTS. There is no significant difference among the experimental groups and the suggested that there is no physiological difference between animals.

During the 5 min after femoral artery incision, the decrease in MAP values in all the injury groups is significantly less than standard gauze; were 47.44 ± 7 mmHg for standard gauze, 66.19 ± 10 mmHg for BC/CTS, 49.46 ± 10 mmHg for SF-coated BC/CTS, 62.87 ± 8 mmHg for SF/PC-coated BC/CTS, 78.99 ± 13 mmHg for SF-coated Kao/BC/CTS, 56.37 ± 8 mmHg for SF-coated Vit K/BC/CTS, and 63.89 ± 10 mmHg for SF-coated PS/BC/CTS. Final MAP values were 73.2 ± 10 mmHg for standard gauze, 69.25 ± 8 mmHg for BC/CTS, 57.38 ± 7 mmHg for SF-coated BC/CTS, 75.11 ± 10 mmHg for SF/PC-coated BC/CTS, 84.26 ± 11 mmHg for SF-coated Kao/BC/CTS, 69.2 ± 11 mmHg for SF-coated Vit K/BC/CTS, and 73.49 ± 12 mmHg for SF-coated PS/BC/CTS. This indicated that the femoral artery-induced blood loss mainly resulted in the decline of MAP. But, stopping bleeding brings the MAP values to the normal.

Blood metabolite values obtained after treatment of hemostatic dressings was given in Table II. The average blood glucose, lactate, and creatinine values for a healthy Sprague–Dawley rat are as follows: 134–219, 0.4–2.2, and 0.1–5.6 mg dL^{-1}, respectively.[40,41] After experiment, the obtained blood lactate and creatinine values are in normal level and but, glucose values at all the groups, especially at SF-coated PS/BC/CTS show a rise compared to normal values. The situation can be interpreted as relationship between PS and blood glucose. Kudriashov *et al.* showed in their study that PS has a resistance to the hypoglycemic effect of insulin.[42]

The average blood gases parameters for a healthy Sprague–Dawley rat are as follows: pH 7.26–7.44, pCO_2 26–54 mmHg, pO_2 93–102 mmHg, 10–89 mmol cSO_2 L^{-1}, and −13.3–1.2 mmol BE (ecf) L^{-1}.[43,44] As shown in Table III, pH values for all the groups are similar and in normal range. The pCO_2 value shows

Table III. Blood Gas Values after Femoral Artery Bleeding Model Created in Healthy Rats

	Gases				
Groups	pH	pCO_2 (mmHg)	pO_2 (mmHg)	BE (ecf) (mM)	cSO_2 (%)
BC/CTS	7.41 ± 0.1	35.9 ± 0.1	121.5 ± 0.3	1.15 ± 0.3	98.25 ± 0.1
SF coated BC/CTS	7.33 ± 0.03	58.6 ± 0.06	85.3 ± 0.9	5.15 ± 1	94.95 ± 0.1
SF/PC coated BC/CTS	7.41 ± 0.07	39.1 ± 0.1	97.4 ± 0.1	2.6 ± 0.1	97.7 ± 0.1
SF coated Kao/BC/CTS	7.356 ± 0.01	47.9 ± 0.9	120 ± 0.7	1.3 ± 0.07	98.4 ± 0.2
SF coated PS/BC/CTS	7.30 ± 0.01	57.4 ± 0.1	91.15 ± 0.3	2.5 ± 0.1	95.9 ± 0.5
SF coated Vit K/BC/CTS	7.37 ± 0.02	44.7 ± 0.1	94 ± 0.1	0.95 ± 0.1	96.8 ± 0.1
Standard gauze	7.3 ± 0.1	44.7 ± 0.1	90.4 ± 0.1	1.7 ± 0.1	96.1 ± 0.3

Table IV. Blood Chemical Values after Femoral Artery Bleeding Model Created in Healthy Rats

	Chemistry					
Groups	Na^+(mM)	K^+ (mM)	Ca^{++} (mM)	Cl^- (mM)	Hct (%)	cHgb (g/dL)
BC/CTS	146.5 ± 0.7	5.1 ± 0.1	1.3 ± 0.1	108.5 ± 0.7	39 ± 0.1	13.2 ± 0.4
SF-coated BC/CTS	143.5 ± 0.1	5.1 ± 0.1	1.26 ± 0.07	103 ± 0.1	40.5 ± 0.5	13.8 ± 0.1
SF/PC-coated BC/CTS	150 ± 0.2	5.25 ± 0.1	1.41 ± 0.07	109 ± 0.1	35 ± 0	11.95 ± 0.07
SF-coated Kao/BC/CTS	145.5 ± 0.3	5.25 ± 0.2	1.38 ± 0.07	107.5 ± 0.3	38.5 ± 0.2	13.05 ± 0.4
SF-coated PS/BC/CTS	145.5 ± 0.1	4.3 ± 0.3	1.37 ± 0.02	104.5 ± 0.7	40 ± 0.2	13.6 ± 0.9
SF-coated Vit K/BC/CTS	145 ± 0.1	4.6 ± 0.3	1.38 ± 0.03	105 ± 0.1	38 ± 0.4	13.1 ± 0.1
Standard gauze	145.5 ± 0.7	4.6 ± 0.6	1.34 ± 0.01	105.5 ± 0.7	38 ± 0.1	12.9 ± 0.5

a slight rise at SF-coated BC/CTS and SF-coated PS/BC/CTS. Extracellular base excess for all the groups are in normal range.

Table IV shows the blood chemistry values after the created femoral artery bleeding model. Normal blood electrolyte values are 142–163 mmol Na^+ L^{-1}, 4.3–5.2 mmol K^+ L^{-1}, 0.27–1.26 mmol Ca^{++} L^{-1}, 101–116 mmol Cl^- L^{-1}, 13–27.1 mmol $cTCO_2$ L^{-1}, Hct (%) 36–44, 12.1–15.9 g cHgb dL^{-1}.[45,46] The obtained electrolyte values are in normal range and the slight rise in Ca^{++} electrolyte concentration is interpreted as Ca^{++} ions released from the hemostatic dressings.

The presence of bleeding at the site after treatment of hemostatic dressings was illustrated in Figure 12. As can be seen in Figure 12(a), the bleeding cannot be stopped after treatment with standard gauze and the injury site is completely filled with blood. This finding demonstrates that standard gauze is ineffective in the femoral artery bleeding model. Figure 12(b) indicates a clear bleeding site after treatment with SF-coated Vit K/BC/CTS.

Histological Examinations. Histologic image of the femoral artery sections stained with HE was given in Figure 13(a–f). Figure 13(a) shows the femoral artery section without treatment of hemostatic dressings. A relatively noninflammatory blood vessel wall structure is seen. Representative section of standard gauze demonstrates inflammation at the both sides of the blood vessel wall. The HE-stained tissue sections of native and coagulative agents-doped hemostatic dressings are presented in Figure 13(c–f). All groups without standard gauze and kaolin-doped BC/CTS hemostatic dressing caused no foreign body reaction around the tissue after treatment. As can be seen in Figure 13(f), there was only a remarkable existence of inflammation in the sections of artery treated with kaolin-doped BC/CTS hemostatic dressing. These data suggested that biological tissue compatibility for native and coagulative agents-doped BC/CTS hemostatic dressings out of kaolin-doped group.

In the literature, there are numerous studies, which report temperature rise, and serious necrosis of tissue at the bleeding site due to exothermic reaction caused by alumina-silicate-based hemostatic agents.[47] The data justified the obtained results.

CONCLUSIONS

We have shown that the native and active agents-doped BC/CTS bilayer hemostatic dressings quickly stop the bleeding in a femoral artery bleeding rat model with low mortality, more

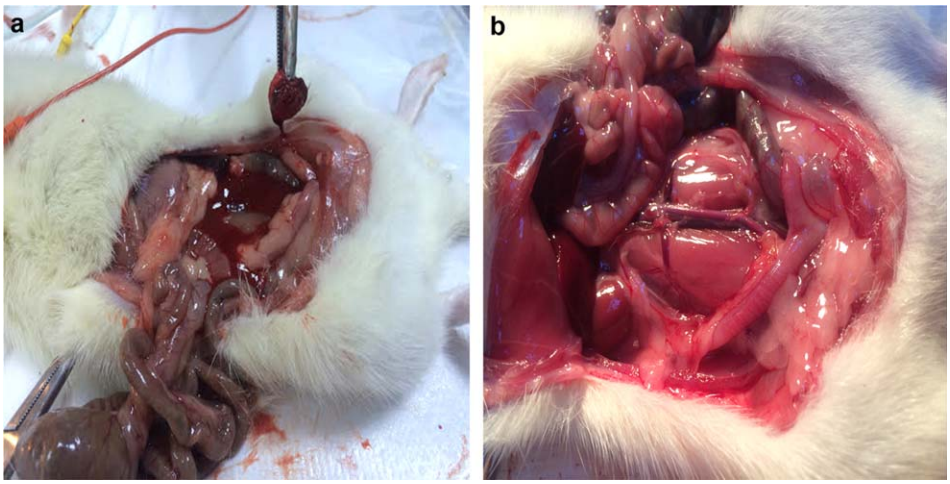

Figure 12. Bleeding site (a) after treatment of standard gauze in a femoral artery rat model and (b) after treatment of SF-coated Vit K/BC/CTS. [Color figure can be viewed in the online issue, which is available at wileyonlinelibrary.com.]

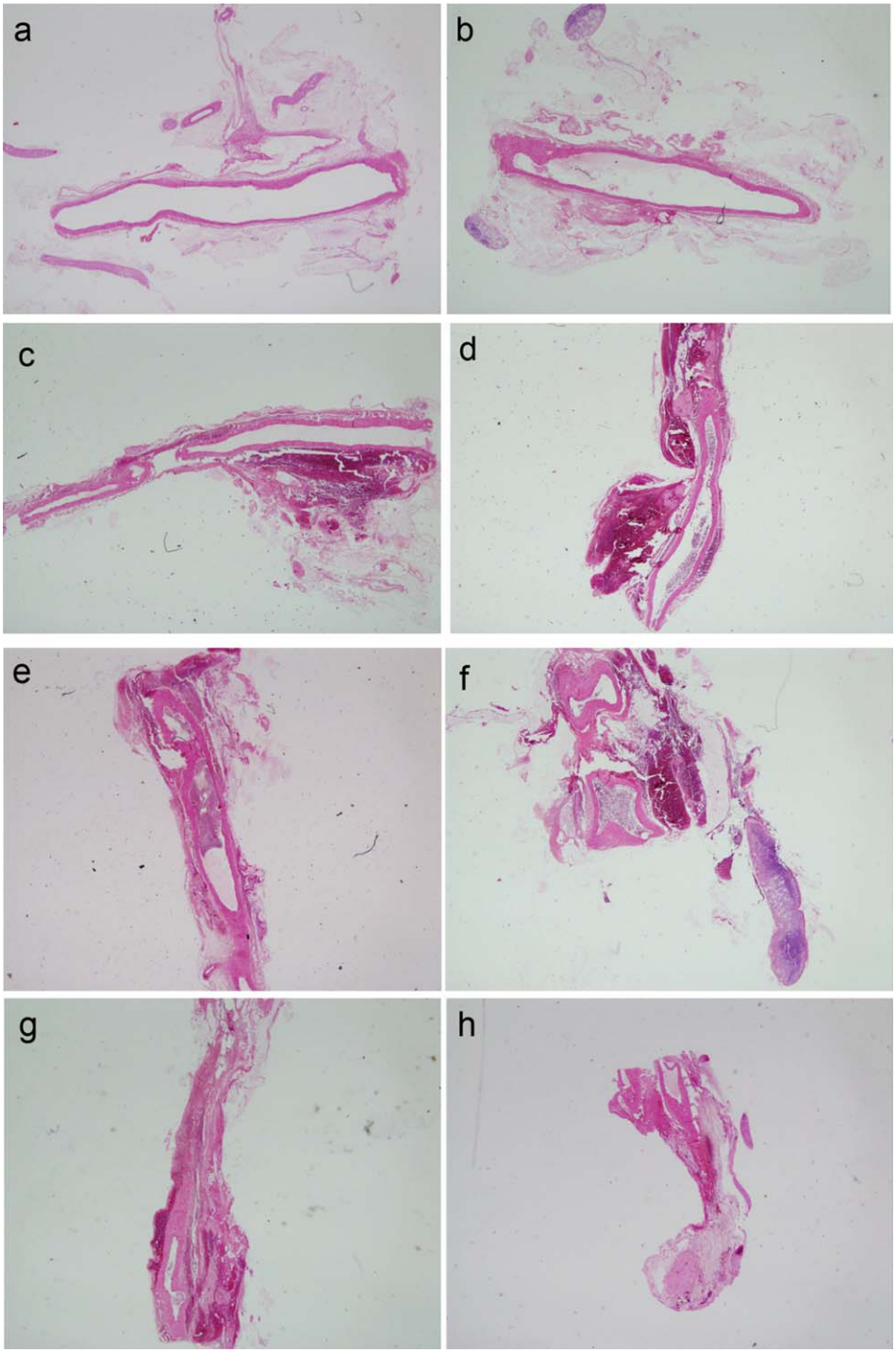

Figure 13. Femoral artery sections stained with hematoxylin–eosin after treatment of hemostatic dressings: (a) control, (b) gauze, (c) BC/CTS, (d) SF-coated BC/CTS, (e) SF/PC-coated BC/CTS, (f) SF-coated Kao/BC/CTS, (g) SF-coated Vit K/BC/CTS, and (h) SF-coated PS/BC/CTS. The fixed tissue samples were stained with hematoxylin–eosin (HE) for microscopic imaging and evaluation. [Color figure can be viewed in the online issue, which is available at wileyonlinelibrary.com.]

platelet activation, reduced tissue reaction, and improved biological tissue compatibility compared to standard gauze. The hemostatic mechanism based on bilayer structure and simultaneous activation of many mechanisms such as absorption of liquid of blood, delivery of coagulation factors, and platelet activation at bleeding site. Our studies show that native or active agent-doped BC/CTS hemostatic dressings can provide an impressive and safe hemostasis for femoral artery bleeding model. An additional important aspect is that the prepared hemostatic dressings can become unique tool for surgeons with ease of handling and low cost as a hemostatic agent.

ACKNOWLEDGMENTS

This work was funded by the Hacettepe University Teaching Staff Training Program Office through a grant "014BIYP604003".

REFERENCES

1. Sauaia, A.; Moore, F. A.; Moore, E. E.; Moser, K. S.; Brennan, R.; Read, R. A.; Pons, P. T. *J. Trauma* **1995**, *38*, 185.
2. Burkatovskaya, M.; Tegos, G. P.; Swietlik, E.; Demidova, T. N.; Castano, A. P.; Hamblin, M. R. *Biomaterials* **2006**, *27*, 4157.
3. Champion, H. R.; Bellamy, R. F.; Roberts, C. P.; Leppaniemi, A. *J. Trauma* **2003**, *54*, 13.
4. Carson, J. L.; Poses, R. M.; Spence, R. K.; Bonavita, G. *Lancet* **1988**, *1*, 727.
5. Wu, W. C.; Trivedi, A.; Friedmann, P. D.; Henderson, W. G.; Smith, T. S.; Poses, R. M.; Uttley, G.; Vezeridis, M.; Eaton, C. B. *Mor. V. Ann. Surg.* **2012**, *255*, 708.
6. Song, H.; Zhang, L.; Zhao, X. *Macromol. Biosci.* **2010**, *10*, 33.
7. Ahlering, T. E.; Eichel, L.; Chou, D.; Skarecky, D. W. *J. Urol.* **2005**, *65*, 994.
8. Levy, O.; Haddo, O.; Sforza, G.; Copeland, S.; Rath, E. *Arthroscopy* **2011**, *27*, 867.
9. Lang, C. J.; Heckmann, J. G.; Neundorfer, B. *J. Neurol. Sci.* **1998**, *160*, 128.
10. Yasunaga, H. *Lancet* **2007**, *370*, 2063.
11. Sahli, H.; Tapon-Bretaudière, J.; Fischer, A. M.; Sternberg, C.; Spenlehauer, G.; Verrecchia, T.; Labarre, D. *Biomaterials* **1997**, *18*, 281.
12. Okamura, Y.; Fukui, Y.; Kabata, K.; Suzuki, H.; Handa, M.; Ikeda, Y.; Takeoka, S. *Bioconjug. Chem.* **2009**, *20*, 1958.
13. Ellis-Behnke, R. G.; Liang, Y. X.; Tay, D. K.; Kau, P. W.; Schneider, G. E.; Zhang, S.; Wu, W.; So, K. F. *Nanomedicine* **2006**, *2*, 207.
14. Dowling, M. B.; Kumar, R.; Keibler, M. A.; Hess, J. R.; Bochicchio, G. V.; Raghavan, S. R. *Biomaterials* **2011**, *32*, 3351.
15. Cheng, T. Y.; Wu, H. C.; Huang, M. Y.; Chang, W. H.; Lee, C. H.; Wang, T. W. *Nanoscale* **2013**, *5*, 2734.
16. Devlin, J. J.; Kircher, S.; Kozen, B. G.; Littlejohn, L. F.; Johnson, A. S. *J. Emerg. Med.* **2011**, *41*, 237.
17. Kozen, B. G.; Kircher, S. J.; Henao, J.; Godinez, F. S.; Johnson, A. S. *Acad. Emerg. Med.* **2008**, *15*, 74.
18. Rhee, P.; Brown, C.; Martin, M.; Salim, A.; Plurad, D.; Green, D.; Chambers, L.; Demetriades, D.; Velmahos, G.; Alam, H. *J. Trauma* **2008**, *64*, 1093.
19. Alam, H.; Burris, D.; DaCorta, J. *Mil. Med.* **2005**, *170*, 63.
20. Gegel, B. T.; Austin, P. N.; Johnson, A. D. *AANA J.* **2013**, *81*, 453.
21. Vogler, E. A.; Graper, J. C.; Harper, G. R.; Sugg, H. W.; Lander, L. M.; Brittain, W. J. *J. Biomed. Mater. Res.* **1995**, *29*, 1005.
22. Hestrin, S.; Schramm, M. *Biochem. J.* **1954**, *58*, 345.
23. Sun, D.; Yang, J.; Wang, X. *Nanoscale* **2010**, *2*, 287.
24. Kim, J.; Cai, Z.; Lee, H. S.; Choi, G. S.; Lee, D. H.; Jo, C. *J. Polym. Res.* **2010**, *18*, 739.
25. Fan, Z. H.; Xie, Z. G.; Zuo, B. Q.; Zhang, P.; Li, L. B.; Shen, Y. X.; Zhang, H. X. *Adv. Mater. Res.* **2011**, *175–176*, 224.
26. Fan, Z.; Shen, Y.; Zhang, F.; Zuo, B.; Lu, Q.; Wu, P.; Xie, Z.; Dong, Q.; Zhang, H. *Cell Transplant.* **2013**, *22 Suppl 1*, S39.
27. McKee, M. G. *Science* **2006**, *311*, 353.
28. Hu, X.; Kaplan, D.; Cebe, P. *Macromolecules* **2006**, *39*, 6161.
29. Nzai, J. M.; Proctor, A. *J. Am. Oil Chem. Soc.* **1999**, *76*, 61.
30. Hu, G.; Xiao, L.; Tong, P.; Bi, D.; Wang, H.; Ma, H.; Zhu, G.; Liu, H. *Int. J. Nanomed.* **2012**, *7*, 2613.
31. Darmoc, M. M.; Lauren, S. B.; Raynor, J. E.; Chou, A.; Cohen, A. (Orthovita Inc.) U.S. Patent 0,230,977 (**2012**).
32. Dai, C.; Yuan, Y.; Liu, C.; Wei, J.; Hong, H.; Li, X.; Pan, X. *Biomaterials* **2009**, *30*, 5364.
33. Henderson, P. W.; Kadouch, D. J. M.; Singh, S. P.; Zawaneh, P. N.; Weiser, J.; Yazdi, S.; Weinstein, A.; Krotscheck, U.; Wechsler, B.; Putnam, D.; Spector, J. A. *J. Biomed. Mater. Res. A* **2010**, *9999A*, NA.
34. Sönmez, E.; Cavuş, U. Y.; Civelek, C.; Dur, A.; Karayel, E.; Gülen, B.; Uysal, O.; Ipek, G. *Ulus Trauma Acil. Cerrahi. Derg.* **2014**, *20*, 79.
35. Nur, I.; Timmorim, M.; Sheetrit, E.; Shoam, I. L.; Liliana, B.; Rehovot, I. L.; Tomer, G.; Modiin, I. L. (Omrix Biopharmaceuticals Ltd.) U.S. Patent 8,475,812, 2015 (**2013**).
36. Bennett, B. L.; Littlejohn, L. F.; Kheirabadi, B. S.; Butler, F. K.; Kotwal, R. S.; Dubick, M. A.; Bailey, J. A. *J. Spec. Oper. Med.* **2014**, *14*, 40.
37. Letourneau, P. A.; Mcmanus, M.; Sowards, K.; Wang, W.; Wang, Y.; Matijevic, N.; Pati, S.; Wade, C. E.; Holcomb, J. B. *J. Trauma* **2011**, *71*, 1115.
38. Wright, J. K.; Kalns, J.; Wolf, E. A.; Traweek, F.; Schwarz, S.; Loeffler, C. K.; Synder, W.; Yantis, L. D.; Eggers, J. *J. Trauma* **2004**, *57*, 224.
39. Arnaud, F.; Tomori, T.; Carr, W.; McKeague, A.; Teranishi, K.; Prusaczyk, K.; McCarron, R. *Ann. Biomed. Eng.* **2008**, *36*, 1708.
40. Sari, D. N.; Endardjo, S.; Santoso, D. I. S. *Med. J. Indonesia* **2013**, *22*, 141.
41. Chin, B. H.; Kozbelt, S. H.; Sullivan, L. *J. Toxicol. Pathol.* **1979**, *7*, 10.
42. Kudriashov, B. A.; Shapiro, B. F.; Ul'ianov, A. M. *Pytel'lu a. Probl Endokrinol (Mosk)* **1984**, *30*, 51.
43. Baker, D. E. In: The Laboratory Rat, Biology and Diseases. I; Baker, H. J., Lindsey, J. R., Weisbroth, S. H., Eds.; Academic Press: New York, **1979**; p 154.
44. Uribe-Escamilla, R.; Aparicio, P. S.; Izquierdo, A. C.; Alfaro-Rodríguez, A. *Multiciencias* **2011**, *11*, 378.
45. Matsuzawa, T.; Hayashi, Y.; Nomura, M.; Unno, T.; Igarashi, T.; Furuya, T.; Sekita, K.; Ono, A.; Kurokawa, Y. *J. Toxicol. Sci.* **1997**, *22*, 25.
46. Alemán, C. L.; Más, R. M.; Rodeiro, I.; Noa, M.; Hernández, C.; Menéndez, R.; Gámez, R. *Lab. Anim.* **1998**, *32*, 457.
47. Li, Y.; Li, H.; Xiao, L.; Zhou, L.; Shentu, J.; Zhang, X.; Fan, J. *Materials* **2012**, *5*, 2586.